Structure of an Exploding Laser-Produced Plasma

A. Collette* and W. Gekelman†

Department of Physics and Astronomy, University of California, Los Angeles, Los Angeles, California 90095, USA

(Received 28 April 2010; published 1 November 2010)

We describe the first-ever volumetric, time-resolved measurements performed with a moving probe within an expanding dense plasma, embedded in a background magnetized plasma. High-resolution probe measurements of the magnetic field and floating potential in multiple 2D cut planes combined with a 1 Hz laser system reveal complex three-dimensional current systems within the expanding plasma. Static ($\omega_{\mathrm{real}} = 0$) flutelike density striations are observed at the leading edge of the plasma, which are correlated to variations in the current layer at the edge of the expanding plasma.

DOI: 10.1103/PhysRevLett.105.195003 PACS numbers: 52.72.+v, 52.35.Py

The expansion of dense plasmas across a magnetic field is a topic of intense interest across a wide variety of disciplines within plasma physics, with applications to solar [1] and magnetospheric [2,3] physics, astrophysics [4], and pellet injection for tokamak refueling [5]. In particular, sub-Alfvénic expansions with length scales comparable to an ion gyroradius are known to exhibit complex behavior, including the formation of current systems which locally reduce the background field (a diamagnetic cavity or ''magnetic bubble''), and large ($\frac{\Delta n}{n} \sim 1$) field-aligned density striations. Space-borne chemical releases [2,3] to study plasma expansion *in situ* within Earth's magnetosphere found large-scale structuring and wave activity [6]. Fast photography of expanding plasmas in laboratory experiments [7–9] found flute modes which grow rapidly at the plasma surface; the origin of these instabilities has been the focus of intensive theoretical investigation [10,11]. Laboratory work also indicates that an expanding plasma can transfer energy to a background plasma in the form of Alfvén waves [12,13], and that the presence of a surrounding plasma may affect how the expansion evolves [9].

In this Letter we describe direct probe-based measurement of an expanding laser-produced plasma, diamagnetic cavity, current systems and related instabilities. Measurements of magnetic field and floating potential are acquired over multiple 2D cut planes totaling over 6000 spatial locations. This large ensemble allows mapping of the spatial structure of the flute modes, along with direct computation of the 3D current density within the expanding plasma.

Figure 1 shows the experimental arrangement. The fundamental concept is a high rep-rate (1 Hz) laser-driven expansion occurring within a large magnetized background plasma, diagnosed by movable probes. The experimental environment ($n = 1 \times 10^{12}$ cm^{-3}, $B_0 = 600$ G, $r_{\mathrm{plasma}} = 60$ cm, $L_{\mathrm{plasma}} = 16$ m) is provided by the Large Plasma Device (LaPD) at UCLA. The LaPD plasma is generated via a highly repeatable pulsed discharge from a biased barium-oxide coated cathode [14], operating at a 1 Hz rep rate. The expanding plasma is formed by laser ablation of a solid cylindrical carbon target, suspended vertically within the LaPD plasma column. A Nd:YAG laser (1.2 J, 10 ns Gaussian) synchronized to the 1 Hz repetition rate of the LaPD background plasma is focused to an 0.5 mm spot on the carbon cylinder ($\phi = 10^{11}$ W/cm^2). A blowoff plasma with initial $n \sim 10^{15}$ cm^{-3} expands across the background field.

The 1 Hz rep rate of the experiment, combined with good shot-to-shot reproducibility, allows direct measurement of quantities within the plasma via movable probes mounted on a novel in-plasma 2D probe drive system [15]. The experiment is performed repeatedly while the probe heads move from place to place in a predetermined pattern. We use both fast ($f_{\mathrm{max}} > 50$ MHz) three-axis magnetic coil probes ($\frac{dB_{x,y,z}}{dt}$) and Langmuir probes configured to measure ac floating potential. The magnetic probes are 1 mm in size (compared to the 4 cm laser plasma), and use differential windings to eliminate electrostatic pickup. The Langmuir probes consist of four 0.5 mm by 0.13 mm tips, two aligned with B and two transverse, embedded in a 1 mm diameter ceramic tube. They are set up to measure high-frequency floating potentials; the tips are grounded to the background plasma column through a 50 Ω resistor. A single fixed-position floating probe is also placed in the machine alongside the moving probes. In combination with a large ensemble of shots, this configuration makes possible [16] the reconstruction of 2D phase patterns associated with phenomena which are not phase-locked shot to shot. An image-intensified CCD camera with a 10 ns shutter is also used to observe the plasma [Fig. 2(a)].

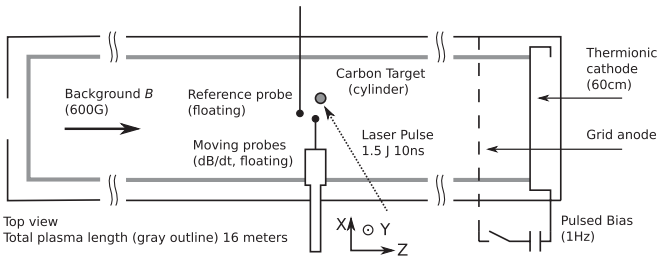

FIG. 1. Experimental setup.

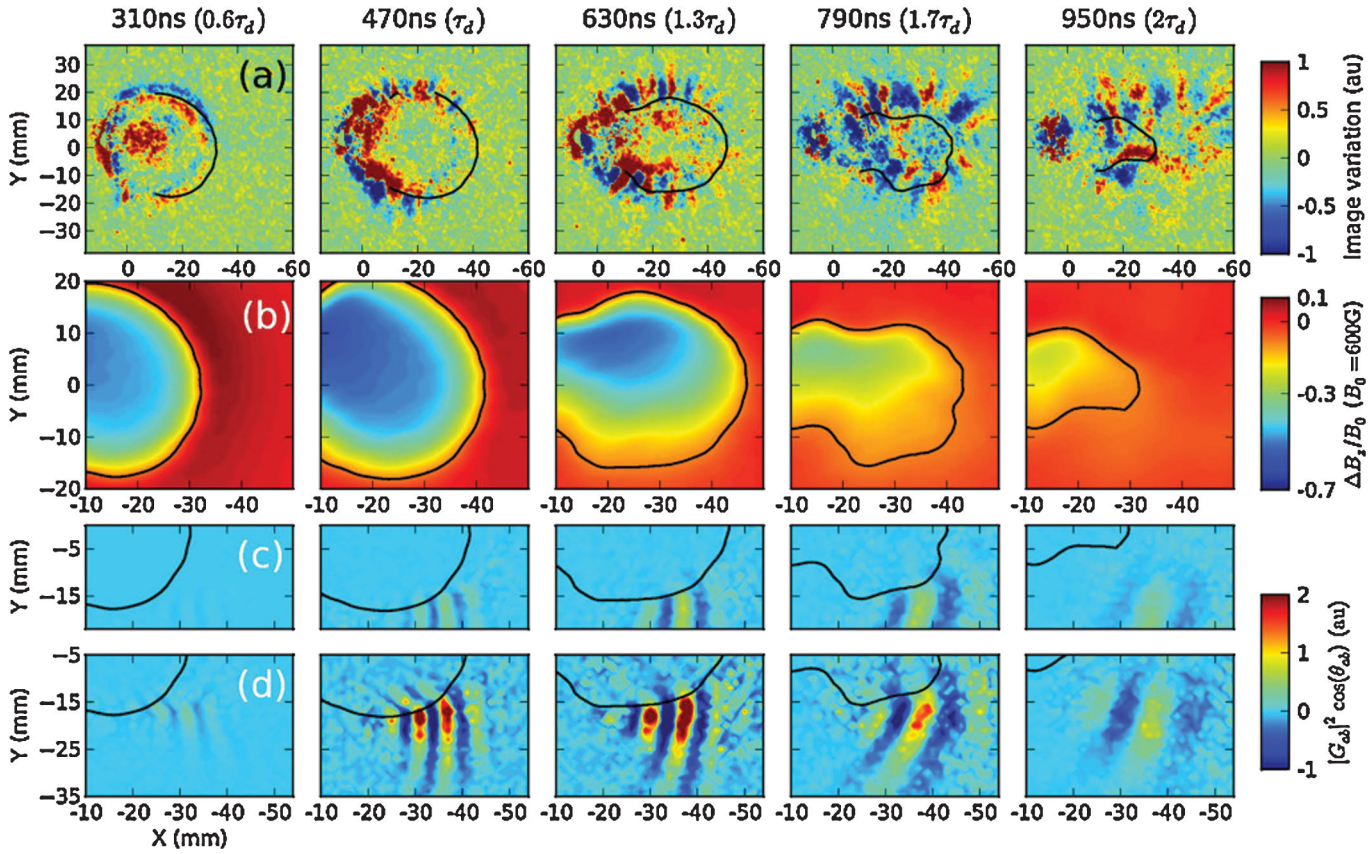

FIG. 2 (color). Time evolution of diamagnetic cavity and flutes, as measured via (a) fast photography, (b) magnetic probes, (c) probe correlation measurements of floating potential, and (d) probe correlation measurements of floating potential with B_z. Solid contour is $\Delta B_z = -50$ G, provided as a reference. Correlation quantity (c),(d) is the real part of the cross-spectral function $G_{ab}(f)$, evaluated at the frequency f where the coherency $\gamma_{ab}(f)$ is maximized for the given time.

Figure 2(b) shows the time evolution of the Z component of the magnetic field, as measured in an XY cut plane 1 cm from the target. The basic mechanism which governs the magnetic field behavior is well understood [17]. The system scale size L satisfies $\rho_e \ll L \lesssim \rho_i$, an asymmetry which leads to charge separation: as the plasma expands, the fast ions outrun the magnetized electrons, resulting in a net radial electric field E_r. Electrons at the inside of the expanding shell then develop an $\mathbf{E}_r \times \mathbf{B}_z$ drift v_ϕ. This poloidal current reinforces the pressure-driven ($\nabla P \times \mathbf{B}$) diamagnetic currents which arise at the density gradient at the front of the expanding plasma. The result is a local reduction in the background field, referred to as a diamagnetic cavity. Natural time and length scales for the expansion are set by the time τ_d taken to reach peak $|B|^2$ (here 470 ns), and the "magnetic confinement radius" R_B reached by the expanding cavity at this time (2 cm). The decay of the magnetic field [Figs. 2(b) and 3] is very rapid, taking 500 ns to reach 10% of its peak value—much faster than the expected magnetic diffusion time (~ 100 μs). Shot-to-shot variation within the plane of Fig. 2 introduces an average experimental uncertainty of 7% for points with $|B| > 0.1|B|_{\text{peak}}$.

Figure 2(a) shows the structures which develop at the edge of the expanding cavity. This time series is assembled from photographs collected with a fast (10 ns shutter) CCD camera oriented along z. At each time step, an ensemble of 10 photographs is taken, and the mean of the ensemble subtracted from each. The displayed 2D pattern corresponds to the variable part of the image. Since the image of the bubble is integrated over z, the visible structures can have no (or small) z dependence and are identified as flutes, similar to those in Refs. [7–9].

We measure these structures by direct observation of the ac floating potential. A Langmuir probe placed in the cut plane of Fig. 2(b) records oscillation bursts as the cavity expands. Correlating the signals from multiple probes [18] allows us to investigate the spatial patterns associated with these time signals. In addition to the moving probe a which maps out the cut plane, a reference probe b is placed at fixed location $x = -35$, $y = -20$. We collect an ensemble of 20 time series at each spatial location, subtract the mean from each time series, and then use the ensemble to calculate the cross-spectral density [19] $G_{ab}(f, x, y, t) = |G_{ab}|e^{-i\theta_{ab}}$, as a function of frequency, position, and time. The behavior of the cross-phase $\theta_{ab}(f, x, y, t)$ versus x and y at a given time and frequency then provides information on the structures' 2D pattern in the quantities measured. In combination with autospectral densities G_{aa} and G_{bb} we can also compute the coherency $\gamma_{ab} = |G_{ab}|/\sqrt{G_{aa}G_{bb}}$, which indicates the degree to which processes on the two probes are correlated.

Correlation measurements were performed between two floating probes [Fig. 2(c)], and between one fixed floating and one moving magnetic coil probe [Fig. 2(d)]. The autospectra of both moving probes reveals a frequency falloff over time from a maximum of 25 MHz at τ_d to less than 10 MHz by $2\tau_d$ [Fig. 4]. Because of the mechanism by which the oscillations are produced, the frequency information is redundant. If we denote as $\lambda_x(f, t)$ the recovered wavelength in x at a given frequency $f(t)$, computation of the quantity $v_{x,\text{effective}} = f\lambda_x$ reveals a near-constant value of 5×10^6 $\frac{\text{cm}}{\text{sec}}$. Figure 3 (open circles) shows this quantity as a function of time. Comparing this value to the final data points for $v_\perp$ (filled circles) derived from following the magnetic field, it appears that the sole source of the time oscillations is the translation of static ($\omega_{\text{real}} = 0$) structures past the diagnostics. The 2D patterns displayed in Figs. 2(c) and 2(d) are chosen by finding the frequency which maximizes the coherency $\gamma_{ab}(f)$ at the given time step.

The 2D structure of the floating correlation measurement strongly resembles the flutes visible via fast photography; the wavelength of the most-coherent mode increases with time, until it is comparable to the system size. The autospectrum of the magnetic field fluctuations [Fig. 4(b)] exhibits the same frequency falloff with time as the floating potential fluctuations. It is reasonable to conclude that in the same way that the floating potential oscillations are caused by the translation of the flutes past the probe, the magnetic field oscillations are caused by spatial variations in the diamagnetic current density. Figure 2(d) shows the 2D correlation between floating potential and the magnetic field oscillations. The pattern is nearly identical to that of the visible flutes and the floating potential correlations, except at the outer edge of the current layer. Here the correlation pattern extends into the diamagnetic current layer, exhibiting a phase change at the boundary, a behavior not observed in the floating potential correlation.

The photograph series and correlation measurements indicate flute formation beginning relatively late in the expansion (after about $0.5\tau_d$). This is consistent with the existence of a critical radius for instability onset [20], although the theoretical estimate in a slab model for our parameters gives $R_c \geq 30$ cm, much larger than the observed magnetic confinement radius $R_B = 2$ cm. Once formed, the flutes grow rapidly; their size is comparable to R_B by τ_d. The wavelength of the flutes also grows from an initial value of 3 mm at τ_d to more than 10 mm at $2\tau_d$.

We are unable to observe a linear regime in either the fast photographs or correlation measurements; as soon as the structures are visible via either method, their length is already comparable to their spacing along the cavity surface, and to the width of the diamagnetic current layer [Fig. 5]. This implies a maximum growth time of less than 20 ns, the time spacing of the fast photograph series. Previous theoretical descriptions of this phenomenon [20] identify it variously as the large-Larmor radius Rayleigh-Taylor (LLR) or lower-hybrid drift instability. In the case of the LLR description, deceleration as the plasma expands provides an effective gravitational force. Figure 3 shows the time behavior of both the magnetic energy $\int \frac{|B|^2}{2\mu_0} dV$ within our measurement volume and the cross-field expansion speed of the cavity. The cavity slows from an initial $v_\perp > 1.5 \times 10^7$ $\frac{\text{cm}}{\text{sec}}$ to $v_\perp = 5 \times 10^6$ $\frac{\text{cm}}{\text{sec}}$ by τ_d, giving a measured value for $g = 3 \times 10^{13}$ $\frac{\text{cm}}{\text{sec}^2}$. Combined with an estimate for the gradient scale length $\{L_n \equiv [\partial \ln(n)/\partial x]^{-1}\}$ from fast photography, this allows an estimate for the LLR growth rate in the short-wavelength regime ($kL_n \gg 1$): $\gamma_{\text{LLR}} = kL_n\sqrt{(g/L_n)}$ (Eq. 4 of Ripin [20]). The resulting theoretical growth time of 525 ns for $\lambda = 3$ mm is much longer than the experimentally derived upper limit.

Measuring all three components of $\mathbf{B}$ over a volume allows direct computation of the currents within the expanding plasma, via $\mathbf{J} = \frac{1}{\mu_0}(\nabla \times \mathbf{B})$. Figure 5 shows the results of this calculation, performed over three cut planes taken at $z = -10$, -15, and -20 mm, with the laser spot at $z = 0$. A strong vertical asymmetry exists in the

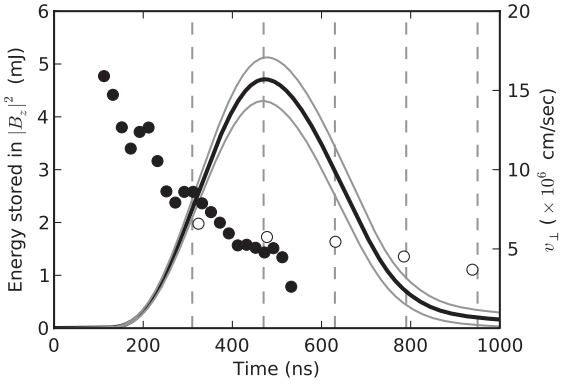

FIG. 3. Cross-field expansion of magnetic cavity. Solid line is energy stored in $|\Delta B_z|^2$ in measured volume ($\sim 10\%$ cavity volume); bounding lines show effect of experimental variation. Closed circles are cross-field expansion speed $v_\perp$ of diamagnetic cavity leading edge; open circles are $f\lambda_x$ from correlation measurements. Vertical marks correspond to the times in Fig. 2.

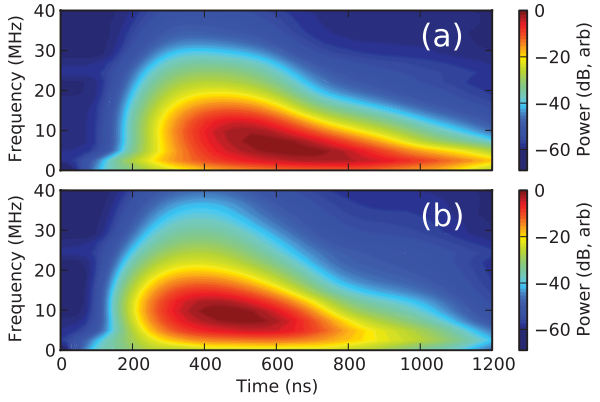

FIG. 4 (color). Autospectra of probe signals in (a) ac floating potential and (b) magnetic field. The power is averaged over a small patch in the region of the reference probe ($x = -35$, $y = -20$), where the oscillations are observed.

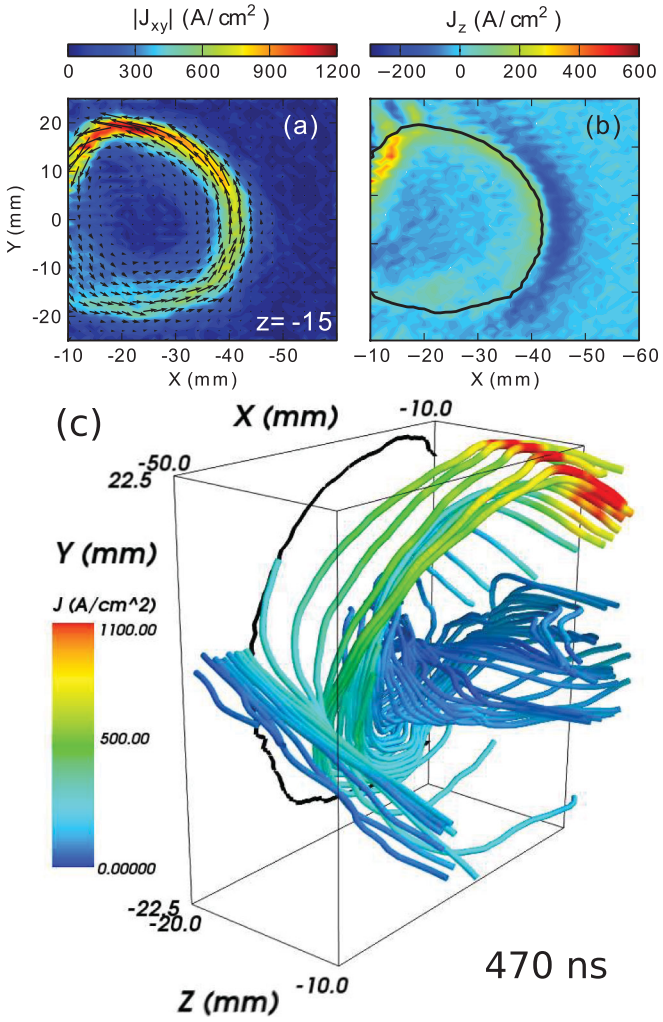

FIG. 5 (color). Three-dimensional currents inside the cavity at τ_d, measured via three cut planes of magnetic field ($z = -10$, -15, -20 mm). Current density is shown in (a) the perpendicular (J_{xy}) and (b) parallel (J_z) directions for the cut plane at $z = -15$ mm, and in streamlines (c) which pass through the line at $z = -15$, $y = 0$. Black contour in all plots is $B_z = -50$ G, as in Fig. 2.

diamagnetic current density J_{xy} [Fig. 5(a)]. At the time of peak diamagnetism, the maximum current density on the top of the cavity is above 1200 A/cm^2, while on the bottom half it is only 500 A/cm^2. Shot-to-shot variation in $\mathbf{B}$ within the plane of Figs. 5(a) and 5(b) results in an average uncertainty in $|\mathbf{J}|$ of 27% for locations with $|\mathbf{J}| > 0.1|\mathbf{J}|_{\text{peak}}$. Computation of the axial current density J_z [Fig. 5(b)] reveals a complicated layered current structure at the edge of the cavity, with magnitudes comparable to that of the diamagnetic current ($|J_z| \sim 0.5|J_{xy}|$). The current layer visible in (a) has a strong component in the $+\hat{z}$ direction in addition to its $\hat{\phi}$ component, while the regions outside the current layer and close to the cavity center acquires a $-\hat{z}$ component of similar magnitude. Visualizing the currents as streamlines [Fig. 5(c)] makes this structure clear; the diamagnetic current flows along z as well as ϕ, in the opposite direction to the currents nearer the center of the cavity. The current outside is directed along $-\hat{z}$ but does not spiral.

In conclusion, we have performed detailed probe measurements of an expanding plasma and associated current systems over a series of 2D cut planes. The data reveal static field-aligned density striations which are correlated to inhomogeneities in the diamagnetic current density, with growth rates much faster than those predicted by a simple theoretical model. We also observe strong current layers at the edge of the expanding plasma, oriented along the direction of the background magnetic field. The mechanism by which these currents close is an open question, and likely to depend on the details of the parallel boundary of the diamagnetic cavity.

We acknowledge the expert technical assistance of M. Drandell and M. Nakamoto, and S. Vincena and P. Pribyl for valuable discussions. This work was supported by DOE/NSF as part of research performed at the Basic Plasma Science Facility, UCLA.

*collette@physics.ucla.edu
†gekelman@physics.ucla.edu

[1] B. C. Low, J. Geophys. Res. **106**, 25141 (2001).
[2] G. Haerendel, G. Paschmann, W. Baumjohann, and C. W. Carlson, Nature (London) **320**, 720 (1986).
[3] P. A. Bernhardt, Phys. Fluids B **4**, 2249 (1992).
[4] B. A. Remington, R. P. Drake, H. Takabe, and D. Arnett, Phys. Plasmas **7**, 1641 (2000).
[5] H. R. Strauss and W. Park, Phys. Plasmas **7**, 250 (2000).
[6] R. Bingham, V. D. Shapiro, V. N. Tsytovich, and U. de Angelis *et al.*, Phys. Fluids B **3**, 1728 (1991).
[7] B. H. Ripin, E. A. McLean, C. K. Manka, and C. Pawley *et al.*, Phys. Rev. Lett. **59**, 2299 (1987).
[8] G. Dimonte and L. G. Wiley, Phys. Rev. Lett. **67**, 1755 (1991).
[9] Y. P. Zakharov, V. M. Antonov, E. L. Boyarintsev, and A. V. Melekhov *et al.*, Plasma Phys. Rep. **32**, 183 (2006).
[10] A. B. Hassam and J. D. Huba, Geophys. Res. Lett. **14**, 60 (1987).
[11] J. D. Huba, A. B. Hassam, and D. Winske, Phys. Fluids B **2**, 1676 (1990).
[12] M. VanZeeland, W. Gekelman, S. Vincena, and J. Maggs, Phys. Plasmas **10**, 1243 (2003).
[13] W. Gekelman, A. Collette, and S. Vincena, Phys. Plasmas **14**, 062109 (2007).
[14] D. Leneman, W. Gekelman, and J. Maggs, Rev. Sci. Instrum. **77**, 015108 (2006).
[15] A. Collette and W. Gekelman, Rev. Sci. Instrum. **79**, 083505 (2008).
[16] W. Gekelman and R. L. Stenzel, J. Geophys. Res. **89**, 2715 (1984).
[17] D. Winske, Phys. Fluids B **1**, 1900 (1989).
[18] S. Vincena and W. Gekelman, Phys. Plasmas **13**, 064503 (2006).
[19] J. Bendat and A. Piersol, *Random Data* (John Wiley & Sons, New York, 2000).
[20] B. H. Ripin, J. D. Huba, E. A. McLean, and C. K. Manka *et al.*, Phys. Fluids B **5**, 3491 (1993).